Acta Crystallographica Section F
Structural Biology and Crystallization Communications
ISSN 1744-3091

High-resolution structure of the native histone octamer

Christopher M. Wood,[a]* James M. Nicholson,[b] Stanley J. Lambert,[a] Laurent Chantalat,[c] Colin D. Reynolds[a] and John P. Baldwin[b]

[a]School of Biomolecular Sciences, Liverpool John Moores University, Byrom Street, Liverpool L3 3AF, England, [b]College of Biology and Medicine, CCLRC Daresbury Laboratory, Warrington, Cheshire WA4 4AD, England, and [c]Structural Biology, Galderma R&D, 635 Routes des Lucioles, BP 87F-06902 Sophia Antipolis CEDEX, France

Correspondence e-mail: c.m.wood@livjm.ac.uk

Received 10 March 2005
Accepted 29 April 2005
Online 1 June 2005

PDB Reference: histone octamer, 1tzy, r1tzysf.

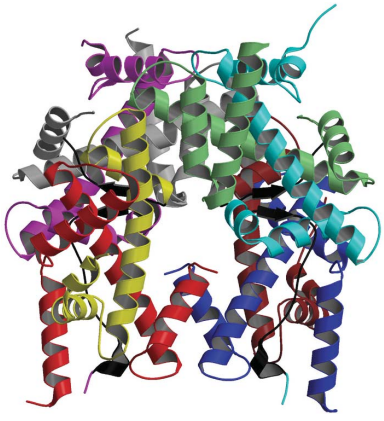

© 2005 International Union of Crystallography
All rights reserved

Crystals of native histone octamers (H2A–H2B)–(H4–H3)–(H3′–H4′)–(H2B′–H2A′) from chick erythrocytes in 2 *M* KCl, 1.35 *M* potassium phosphate pH 6.9 diffract X-rays to 1.90 Å resolution, yielding a structure with an R_{work} value of 18.7% and an R_{free} of 22.2%. The crystal space group is $P6_5$, the asymmetric unit of which contains one complete octamer. This high-resolution model of the histone-core octamer allows further insight into intermolecular interactions, including water molecules, that dock the histone dimers to the tetramer in the nucleosome-core particle and have relevance to nucleosome remodelling. The three key areas analysed are the H2A′–H3–H4 molecular cluster (also H2A–H3′–H4′), the H4–H2B′ interaction (also H4′–H2B) and the H2A′–H4 β-sheet interaction (also H2A–H4′). The latter of these three regions is important to nucleosome remodelling by RNA polymerase II, as it is shown to be a likely core-histone binding site, and its disruption creates an instability in the nucleosome-core particle. A majority of the water molecules in the high-resolution octamer have positions that correlate to similar positions in the high-resolution nucleosome-core particle structure, suggesting that the high-resolution octamer model can be used for comparative studies with the high-resolution nucleosome-core particle.

1. Introduction

The DNA of eukaryotic cell nuclei is packaged into chromatin and, at a higher level, chromosomes by a basic repeating unit known as the nucleosome, a component of which is the nucleosome-core particle (NCP). The NCP consists of 1.65 turns of superhelical DNA wrapped around a structure called the histone octamer (HO; Luger *et al.*, 1997; Harp *et al.*, 2000; Akey & Luger, 2003). The superhelical turns are comprised of 147 base pairs (bp) of DNA that are bound to the basic HO, which is formed from two duplicated sets of four histone proteins H2A, H2B, H3 and H4. The eight histone proteins are arranged as a central tetramer of form (H4–H3)–(H3′–H4′) that is flanked at each side by a (H2A–H2B) dimer to give an overall structure (H2A–H2B)–(H4–H3)–(H3′–H4′)–(H2B′–H2A′) (Fig. 1). One NCP is concatenated with the next by a length of H1 linker histone or its variants that account for an extra species-dependent length of DNA (typically 50 bp; Woolfe, 1999). The structure of the eight core histones is well established (Arents *et al.*, 1991), with each consisting of three α-helices α1, α2 and α3 with loops L1 and L2 spanning the inter-helix regions. These intra-histone protein structural elements associate with each other as a histone fold. In the (H2A–H2B) and (H3–H4) dimers, the two histone folds congregate together to form a histone-fold pair that forms a tightly bound stable unit of hydrophobic interactions and hydrogen bonds. The full HO is formed from the interactions of three four-helix bundles (4HB) between the two (H3–H4) dimers and also between the two (H2A–H2B) dimers and the (H4–H3)–(H3′–H4′) tetramer (see Fig. 2 of Chantalat *et al.*, 2003). The 4HB are not the only regions of the HO that serve to maintain structural integrity; there is also (Fig. 2) a H2A–H3′–H4′ molecular cluster (MC) (and equivalently for H2A′–H3–H4), H2A–H4′ β-sheet docking (BS) (and equivalently for H2A′–H4) and H4′–H2B docking (H42B) (and equivalently for H4–H2B′). Of particular importance is

the BS interaction (black regions in Fig. 1), as disruption thereof by, for example, the mutation Y98G of H4, will instigate a break-up not only of BS but also of MC and H42B, leading to nucleosome disruption (Santisteban *et al.*, 1997).

As condensed chromatin presents an effective barrier to transcription, it is necessary for RNA polymerase II (Pol II) to call on the assistance of elongation factors such as FACT ('facilitates transcription'), which will bind to the H2A–H2B dimer (Orphanides *et al.*, 1998), thereby allowing the removal of a H2A–H2B dimer by NAP1 (nucleosome-assembly protein 1) and the insertion of a dimer variant such as H2A.Z–H2B (Park *et al.*, 2005). In the H2A.Z–H2B dimer variant, residue 104 of H2A is a glycine (Suto *et al.*, 2000), whereas in the present HO model and in the NCP (Luger *et al.*, 1997) this residue is a glutamine that forms three hydrogen bonds that are absent from the H2A.Z variant. These missing hydrogen bonds allow easier disruption of the nucleosome, assisted by relevant elongation factors that are bound to the HO.

Precisely where these compounds bind the HO has so far eluded investigators, but it is now becoming apparent that the HO-binding issue is as important as DNA binding in the NCP. Most work on HO binding has rightly concentrated on the histone tails and it is now known that compounds such as HP1 (heterochromatin protein 1) will specifically bind methylated H3 histone tails (Nielsen *et al.*, 2002), in this case *via* its chromodomain. Since compounds bind to the histone tails, the structure of those tails becomes more relevant, especially as predicted-structure studies suggest that the sites of methylation are in structural regions (Nicholson *et al.*, 2003). The evidence of non-tail binding in histones is less abundant, but is nevertheless present, and it has been shown that during replication the nuclear HAT1 (histone acetyltransferase 1) protein, which is involved in *de novo* nucleosome assembly, will use its P46 subunit to bind H4 in the region of the α1 helix, but not when the H4 is in an NCP (owing to hindrance; Verreault *et al.*, 1997). Here, we hypothesize that the region of the HO that binds elongation factors and other histone-binding compounds involved in transcription is in the BS interaction area. We also show how the HO solvent structure binds and stabilizes DNA-entry points and indicate that the solvent structure herein compares favourably with that of the NCP. The facility of having a HO model at the same resolution as the NCP is of fundamental importance, as it will allow accurate comparative studies in important fields such as transcription and replication.

2. Materials and methods

As in previous studies (Chantalat *et al.*, 2003), chick HOs were prepared in 2 *M* KCl, 0.2 *M* K_2HPO_4, 0.2 *M* KH_2PO_4 and dialysed against 2 *M* KCl, 0.475 *M* K_2HPO_4, 0.475 *M* KH_2PO_4 at 277 K overnight with two changes of buffer and centrifuged at 13 000*g* for 1 h. The supernatant containing pure HOs was concentrated to 20 mg ml^{-1} (OD_{278} = 9), partitioned into 50 µl crystallization cells and dialysed against 10 ml 2 *M* KCl, 0.675 *M* K_2HPO_4, 0.675 *M* KH_2PO_4 to cystallize. Solutions made up from anhydrous KCl and phosphates were the conditions that gave the best crystals, including that used in this study. A range of crystallization buffer pH values were prepared by changing the ratios of monobasic to dibasic phosphate ions by small variations around the two 0.675 *M* values, keeping the total phosphate concentration at 1.35 *M*. This gave a range of samples covering a pH window centred on 6.9. After a few weeks, large 2–3 mm long crystal needles had grown. The resulting HO crystals, grown in the absence of reducing or oxidizing agents, were hexagonal, space group $P6_5$, with unit-cell parameters $a = b = 158.7$, $c = 103.6$ Å and one octamer in the asymmetric unit (Chantalat *et al.*, 2003; Lambert *et al.*, 1999).

Prior to data collection, the crystals were removed from the dialysis cells on loops of fine-stranded unwaxed dental floss. The crystals were soaked for 10 s in 2 *M* KCl, 0.675 *M* K_2HPO_4, 0.675 *M* KH_2PO_4, 10% glycerol and for 10 s in the same buffer containing 15% glycerol and then 20% glycerol. They were then introduced directly into liquid nitrogen and finally placed in the 100 K cryostream of the X-ray diffractometer for data acquisition.

Data were collected on beamline 14.2 of the CCLRC Daresbury Laboratory Synchrotron Radiation Source using an ADSC Q4 CCD detector. The data were processed using the *HKL* program suite (Otwinowski & Minor, 1997), yielding an overall merging *R* value of 8.9% and a value of 37.7% in the 1.95–1.90 Å highest resolution shell. In all, 115 923 unique reflections were recorded, corresponding to a completeness of 99.9% overall and 98.5% in the highest resolution shell, with a multiplicity of 5.4 (3.5 in the highest resolution shell) and a mosaicity in the range 0.35–0.48°. The percentage of reflections with $I > 3\sigma(I)$ was 94.5% (84.6% in the highest resolution shell).

The structure was solved using the 2.15 Å model of the HO (PDB code 1hq3) as a search model. The 1.90 Å model data were collected

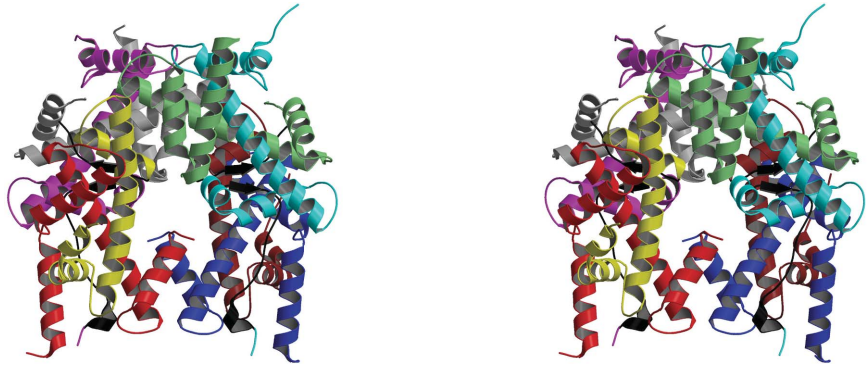

Figure 1
Stereo image showing the 1.90 Å octamer (PDB code 1tzy). The colour coding is H2A, cyan; H2B, light green; H3, red; H4, yellow; H2A′, magenta; H2B′, grey; H3′, blue; H4′, brown. The H2A–H4′ and H2A′–H4 docking regions are shown in black.

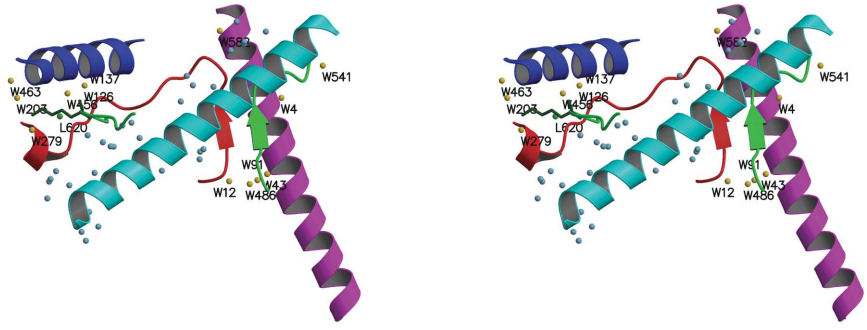

Figure 2
Stereo image showing BS, MC and H42B interaction regions. The colour code is red for the H2A docking sequence; green for the H4′ docking sequence; blue for the H3′ αN helix; magenta for the H2B α2 helix; cyan for the α2 H3′ helix; gold for those waters associated with the docking sequences; sky blue for those waters involved in holding the α2 H3′ helix within the molecular cluster; lime green for chloride L620; dark green for Lys44 of H4′.

as an independent data set, with none of the lower resolution model structure factors being used. The model development was carried out using the *AMoRe* program (Navaza, 1994) and refinement used the program *REFMAC5* (Murshudov *et al.*, 1997). Both of these and subsequent programs were used within the *CCP*4 crystallographic package (Collaborative Computational Project, Number 4, 1994). Model building and refinement initially involved only the residues of the search model.

Rigid-body refinement for four cycles resulted in a value of 27.4% for R_{work} and of 27.7% for R_{free}. Five cycles of TLS refinement brought these values down to 24% for R_{work} and 25.68% for R_{free}. The structure was then observed in *O* (Jones *et al.*, 1991) on a residue-by-residue basis using $2F_o - F_c$ and $F_o - F_c$ maps. Positions of missing phosphate and chloride ions were clearly visible and these were manually inserted into the appropriate positions. After further refinement, waters were added using the *ARP*/*wARP* program (Lamzin & Wilson, 1993). Waters were added in cycles of 35 at a time, with a refinement at the end of each cycle, for a total of 30 cyles. A water was kept if above 3σ in the $F_o - F_c$ map and rejected if below 1σ in the $2F_o - F_c$ map. A total of 612 waters were included in the final model, which resulted in a final value of 18.7% for R_{work} and of 22.2% for R_{free}. The solvent content of the final model is 69.33%, giving a Matthews coefficient of 4.04 Å^3 Da^{-1}. All residues either fell into the most favoured (96%) or the allowed (4%) areas of the Ramachandran plot (Ramachandran *et al.*, 1963). Table 1 gives a summary of the data-collection and final refinement statistics.

Table 1
Data-collection and refinement statistics.

Values in parentheses refer to the highest resolution shell (1.90–1.95 Å).

Crystal dimensions (mm)	20 × 0.25 × 0.25
X-ray source	Station 14.2, SRS Daresbury, UK
Detector	ADSC Q4 CCD
Wavelength (Å)	0.98
Temperature (K)	100
Rotation range (°)	0–109.2
Rotation step (°)	0.35
Space group	$P6_5$
Unit-cell parameters (Å)	$a = b = 158.701$, $c = 103.635$
Resolution (Å)	30.0–1.90
Mosaicity (°)	0.35–0.48
Total reflections	613452
Unique reflections	115923
Merging *R* factor (%)	8.9 (37.7)
Completeness (%)	99.9 (98.5)
Reflections with $I > 3\sigma(I)$ (%)	94.5 (84.6)
Multiplicity	5.4 (3.5)
R_{work} (%)	18.7
R_{free} (%)	22.2
No. of protein atoms	5985
No. of solvent atoms	612
No. of heteroatoms	28
R..m.s. deviations from ideal geometry	
Bonds (Å)	0.02
Angles (°)	1.9
Improper angles (°)	1.1
Torsion angles (°)	5.9
Estimated coordinate error	
Luzzati plot (Å)	0.23
σ_A plot (Å)	0.21
Ramachandran plot	
Most favoured (%)	96
Allowed (%)	4
Average *B* factors (Å^2)	
Overall protein atoms	46.1
Main-chain protein atoms	42.3
Side-chain protein atoms	48.4
Water	56.1
Phosphates	75.7
Chlorides	52.1

3. Results

3.1. Alignment of the HO and NCP high-resolution structures

For an effective comparison of the present structure with that of the NCP, the H2A and H2A′ docking sequences of the NCP (residues Gly98–Leu116) were aligned to the H2A and H2A′ docking sequences of the HO (residues Gly98–Leu116) using *LSQKAB* (Kabsch, 1976). An HO water was deemed to be equivalent to an NCP water if it was within half a hydrogen-bond distance. To clearly distinguish between HO and NCP water molecules, references to the former are in normal text, whilst those to the latter are italicized. Although the HO and NCP models (Luger *et al.*, 1997) do not use the 'W' chain letter for their waters, it is used here for consistency. Any water in parentheses is in the same position (previously defined) as the water immediately preceding it.

3.2. Functional aspects of the MC regions

This small molecular cluster has an important role in octamer/DNA stability, since it guides the DNA into (and out of) the NCP. It will be shown how three N-terminal water molecules of the H3′ αN helix form bonds that help to lock in place residue Lys44 of H4′, which is the last residue before the DNA-binding region of the (H3′–H4′) histone fold.

The H3′ αN helix and H2A interact *via* a helix comprised of residues Gln112–Leu116 of H2A that are part of a hydrophobic channel, with Leu48, Ile51 and Gln55 of H3′ on the opposite side. The seven water molecules of the HO involved in hydrogen bonds in this region are W126, W137, W203, W279, W445, W456 and W463 (Fig. 2), of which three, W203, W279 and W463, form the N-terminal water bridge of the H3′ αN helix. This water bridge was not visible in our previous structure of the octamer (Chantalat *et al.*, 2003), but is visible in the NCP (Luger *et al.*, 1997), which is of comparable resolution to the present HO model.

The three waters W203, W279 and W463 bind residue Lys44 of H4′ to the H3′ αN helix and, in so doing, stabilize the DNA-binding region that immediately follows it. The solvent bridge is Thr45 (of H3′)–W463–W203–Lys44 (of H4′)–W279. Since the αN helix of H3′ is securely stabilized by hydrophobic interactions with H2A, the result is a stable entrance point for DNA. The equivalent path in the NCP is Thr45–*W1172*–*W244*–Lys44–*W87*. Waters W203 and W279 of the HO occupy the same positions as waters *W244* and *W87* of the NCP, respectively. Whilst W468 of the HO does not have a water in a duplicate position in the NCP, it is very near to *W1172*.

Although the H2A and H3′ αN region is hydrophobic, there is a rear water bridge (when viewing Fig. 2) that involves chloride ion L620. The bonding path is Arg52 (of H3′)–W137–W126–W456–L620–W445–Asn110 (of H2A). W456 was not resolved in our earlier model (Chantalat *et al.*, 2003) and so the bridge there is incomplete. There is a similar water bridge in the NCP (Luger *et al.*, 1997) that utilizes the waters *W93* (W137), *W19* (W126), *W286* (W456) and *W44* (L620). Whilst W445 of the HO has no NCP water in the same position, *W2528* is near.

3.3. A possible site for core-histone binding

One of the most successful ways of predicting potential ligand-binding sites in a protein is to measure the degree of solvent accessibility of the protein's surface. Since there is also conservation of residues involved in binding sites, we combine these two methods to show that the BS regions (Fig. 2) form the most likely binding site for octamer-modifying compounds. The latter method of residue

conservation has already been examined in detail (Nicholson *et al.*, 2004) and so this section concentrates on showing that the BS regions are capable of binding a ligand in a solvent-excluded space. The method utilized here is a geometric one of surface spheres to determine the cavity and then establishing the proportion of residues in that cavity that are buried (Brady & Stouten, 2000). The binding sites of the BS regions are in addition to but independent of the interaction regions involved in $P6_5$ crystal packing that we identified previously (Chantalat *et al.*, 2003).

Firstly, the cavities of the HO (PDB code 1tzy) were identified using *DEEPVIEW* (Guex & Peitsch, 1997; Fig. 3*a*). All the cavities of the HO were found to congregate around the two docking sequences and of these a majority were close to the two BS regions, with the total volume of the cavities amounting to 240 Å^3. Predicted binding sites were generated (Brady & Stouten, 2000) and their coordinates stored in PDB format, allowing them to be represented graphically as spheres (Fig. 3*b*). The top-ranked binding site (red in Fig. 3*b*) was right in the middle of the two BS regions. To check the accuracy of the predictions, other binding sites were checked to see if they correlated with known DNA/octamer-binding sites and it was found that the DNA minor-groove binding sites of the NCP (Luger *et al.*, 1997) were identified (Fig. 3*b*). For example, the DNA-binding site discussed in the previous section, comprised of residues 45–48 of H4′, was one of those used and was found to be accurately predicted (cyan in Fig. 3*b*). As a further test and since we have emphasized the importance of the solvent structure in the present paper and its influence on binding-site integrity, the predicted binding sites were regenerated but this time ignoring the solvent structure and just using the tertiary residues, phosphates and chlorides. This time, the predicted binding sites were completely different (data not shown) and showed no correlation with known binding sites. Thus, the conclusion from residue conservation (Nicholson *et al.*, 2004) and from cavity and solvent-accessibility analysis is that the most likely octamer-binding site for elongation factors and similar octamer-modifying compounds is in the two BS regions.

The hydrophobic nature of the docking-sequence interactions is clearly visible (Figs. 2 and 4). Nevertheless, there are some key water molecules around the docking regions in both the HO and NCP: W582 (*W2919*) and W43 (*W296*) (Davey *et al.*, 2002). In the HO the N-terminal end of the H2B α2 helix is stabilized by being bound to the H2A docking sequence by water W582 (Fig. 2): Lys57 (of H2B)–W582–Gln104 (of H2A). The identical bridge in the NCP is Lys54 (of H2B)–*W2919*–Gln104 (of H2A). This solvent bridge was not visible in our earlier model of the octamer. In the HO, W43 (*W296*), W12 (*W3*), W91 (*W37*) and W486 (*W125*) are four waters that tie the N-terminal ends of the BS regions to the H2B α2 helix. Another important water in the NCP is *W1727* (Davey *et al.*, 2002). This water is in the same position as chloride L614 in the HO, the function of which is to mediate interaction between Gly101 of H4′ and Ser64 of H2B.

Thus, in both the HO and NCP, there are the same solvent bridges linking the N-terminals of the H2B α2 helix and BS regions, to form a locking-in of the structure.

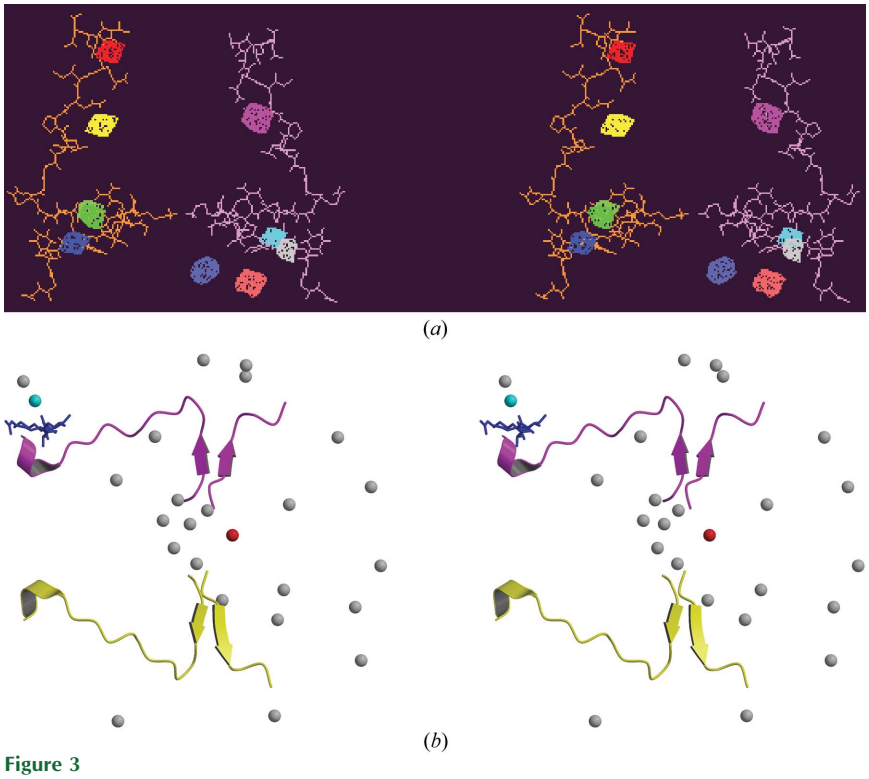

Figure 3
Two stereo images of the binding site. The colour code for (*a*) is orange for the H2A–H4′ docking sequence; magenta for the H2A′–H4 docking sequence and assorted colours for the HO cavities identified by *DEEPVIEW* (Guex & Peitsch, 1997). The total volume for the cavities shown is 240 Å^3. The colour code for (*b*) is magenta for the H2A′–H4 docking sequence and yellow for the H2A–H4′ sequence. Grey spheres are not waters, but the predicted core-histone and DNA-binding sites (Brady & Stouten, 2000). The binding sites have been superimposed onto a ribbon representation of the docking sequences. The red sphere is the top-ranked binding site and falls midway between the two docking regions. The cyan sphere is one of the predicted binding sites used to test the voracity of the predictions and correlates with the actual DNA-binding area shown in blue, which is comprised of residues Arg45, Ile46, Ser47 and Gly48 of H4′ (Chantalat *et al.*, 2003). As a second test, predicted binding sites were regenerated without considering the solvent structure (data not shown). The predicted sites showed no correlation with known binding sites.

3.4. Overview of the HO water structure

Of the 612 waters in the present model, 421 correlate well with waters in the NCP. Even though the HO and NCP models have been produced from different species, by different biochemical processes and by different X-ray diffraction and refinement procedures, the similarity in both solvent and secondary structures is such that the two models can be employed in studies that involve comparisons between the nucleosome, with and without its bound DNA. The solvent structure indicates a preference for the dimers over the tetramer, with each H2A–H2B dimer having 106 directly hydrogen-bonded waters, compared with only 67 for the (H4–H3)–(H3′–H4′) tetramer.

4. Discussion

We have presented a 1.90 Å model of the HO, with an emphasis on explaining how key regions of the structure serve to maintain the overall integrity of the octamer. In particular, we have shown how the solvent structure locks in place key residues such as Lys44 of H4′ which, significantly, is the last residue before the DNA-binding region of residues 45–48 (Chantalat *et al.*, 2003). Using the techniques of residue conservation, cavity analysis and solvent accessibility, we have isolated the probable binding site for compounds that have to bind the core histones during transcription. This mode of binding is distinct from histone-tail binding and from DNA binding.

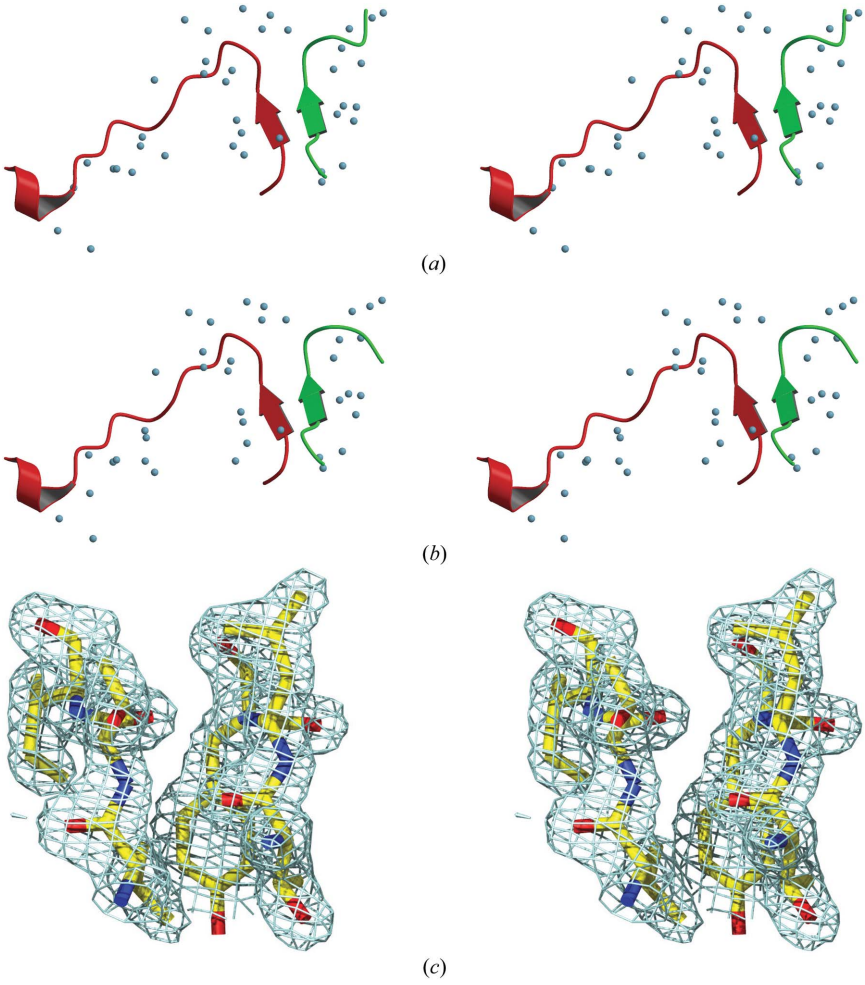

Figure 4
Three stereo images showing the BS regions. The colour code is green for the H4′ docking sequence, red for the H2A docking sequence and sky blue for key waters. (*a*) shows the key waters of the BS region in the HO. (*b*) shows the same area of the NCP after it has been aligned with the HO. Note the good match in water positions between the two figures and the hydrophobic channel between the two docking sequences. This is the primary site (and equivalently the H4–H2A′ docking sequence) that needs to be disrupted before RNA polymerase II-mediated transcription can proceed. (*c*) shows the $2F_o - F_c$ electron density around the BS region (contoured to 3σ, 0.45 e Å^{-3}, values are from *COOT*; Emsley & Cowtan, 2004).

However, the evidence suggests that compounds for which the NCP is a substrate will utilize more than one of these techniques, as for the SPT16-POB3 factor, which is thought to bind DNA *via* the HMG-box domain of POB3 and concurrently the core histones through the acidic C-terminal of SPT16 (Wittmeyer *et al.*, 1999).

During Pol II-mediated transcription, disruption of the nucleosome is required (Kireeva *et al.*, 2002) and this is achieved by Pol II forming a complex with chromatin, where the nucleosomes are deficient in one (H2A–H2B) dimer (Belotserkovskaya & Reinberg, 2004; Baer & Rhodes, 1983). It is suggested that disruption progresses with the breakup of the BS region that in turn causes the MC and H42B areas to dissociate and thereby creates an opening up of the NCP.

This work was supported by John Moores University and forms part of the Daresbury Collaborative Research Program. Structural data were collected on the Biology and Medicine beamline 14.2 at Daresbury. Harrisons Poultry, Antrobus, Cheshire kindly supplied the chicken blood. Figures were produced using *O* (Jones *et al.*, 1991), *MOLSCRIPT* v.2.0 (Kraulis, 1991), *RASTER3D* (Merritt & Bacon, 1997), *MOLRAY* (Harris & Jones, 2001), *DEEPVIEW* (Guex & Peitsh, 1997) and *COOT* (Emsley & Cowtan, 2004).

References

Akey, C. W. & Luger, K. (2003). *Curr. Opin. Struct. Biol.* **13**, 6–14.
Arents, G., Burlingame, R. W., Wang, B.-C., Love, W. E. & Moudrianakis, E. N. (1991). *Proc. Natl Acad. Sci. USA*, **88**, 10148–10152.
Baer, B. W. & Rhodes, D. (1983). *Nature (London)*, **301**, 482–488.
Belotserkovskaya, R. & Reinberg, D. (2004). *Curr. Opin. Genet. Dev.* **14**, 1–8.
Brady, G. P. & Stouten, P. F. W. (2000). *J. Comput.-Aided Mol. Des.* **14**, 383–401.
Chantalat, L., Nicholson, J. M., Lambert, S. J., Reid, A. J., Donovan, M. J., Reynolds, C. D., Wood, C. M. & Baldwin, J. P. (2003). *Acta Cryst.* D**59**, 1395–1407.
Collaborative Computational Project, Number 4 (1994). *Acta Cryst.* D**50**, 760–763.
Davey, C. A., Sargent, D. F., Luger, K., Maeder, A. W. & Richmond, T. J. (2002). *J. Mol. Biol.* **319**, 1097–1113.
Emsley, P. & Cowtan, K. (2004). *Acta Cryst.* D**60**, 2126–2132.
Guex, N. & Peitsch, M. C. (1997). *Electrophoresis*, **18**, 2714–2723.
Harp, J. M., Hanson, B. L., Timm, D. E. & Bunick, G. J. (2000). *Acta Cryst.* D**56**, 1513–1534.
Harris, M. & Jones, T. A. (2001). *Acta Cryst.* D**57**, 1201–1203.
Jones, T. A., Zou, J.-Y., Cowan, S. W. & Kjeldgaard, M. (1991). *Acta Cryst.* A**47**, 110–119.
Kabsch, W. (1976). *Acta Cryst.* A**32**, 922–923.
Kireeva, M. L., Walter, W., Tchernajenko, V., Bondarenko, V., Kashlev, M. & Studitsky, V. M. (2002). *Mol. Cell*, **9**, 841–852.
Kraulis, P. J. (1991). *J. Appl. Cryst.* **24**, 946–950.
Lambert, S. J., Nicholson, J. M., Chantalat, L., Reid, A. J., Donovan, M. J. & Baldwin, J. P. (1999). *Acta Cryst.* D**55**, 1048–1051.
Lamzin, V. S. & Wilson, K. S. (1993). *Acta Cryst.* D**49**, 129–149.
Luger, K., Maeder, A. W., Richmond, R. K., Sargent, D. F. & Richmond, T. J. (1997). *Nature (London)*, **389**, 251–260.
Merritt, E. A. & Bacon, D. J. (1997). *Methods Enzymol.* **277**, 505–524.
Murshudov, G. N., Vagin, A. A. & Dodson, E. J. (1997). *Acta Cryst.* D**53**, 240–255.
Navaza, J. (1994). *Acta Cryst.* A**50**, 157–163.
Nicholson, J. M., Wood, C. M., Reynolds, C. D., Brown, A., Lambert, S. J., Chantalat, L. & Baldwin, J. P. (2004). *Ann. NY. Acad. Sci.* **1030**, 642–653.
Nicholson, J. M., Wood, C. M., Reynolds, C. D., Lambert, S. J., Chantalat, L. & Baldwin, J. P. (2003). *Recent Res. Dev. Mol. Biol.* **1**, 165–187.
Nielsen, P. R., Nietlispach, D. I., Mott, H. R., Callaghan, J., Bannister, A., Kouzarides, T., Murzin, A. G., Murzina, N. V. & Laue, E. D. (2002). *Nature (London)*, **416**, 103–107.
Orphanides, G., LeRoy, G., Chang, C. H., Luse, D. S. & Reinberg, D. (1998). *Cell*, **92**, 105–116.
Otwinowski, Z. & Minor, W. (1997). *Methods Enzymol.* **276**, 307–326.
Park, Y.-J., Chodaparambil, J. V., Bao, Y., McBryant, S. J. & Luger, K. (2005). *J. Biol. Chem.* **280**, 1817–1825.
Ramachandran, G. N., Ramakrishnan, G. & Sasisekhran, V. (1963). *J. Mol. Biol.* **7**, 95–99.
Santisteban, M. S., Arents, G., Moudrianakis, E. N. & Smith, M. M. (1997). *EMBO J.* **16**, 2493–2506.
Suto, R. K., Clarkson, M. J., Tremethick, D. J. & Luger, K. (2000). *Nature Struct. Biol.* **7**, 1121–1124.
Verreault, A., Kaufma, P. D., Kobayashi, R. & Stillman, B. (1997). *Curr. Biol.* **8**, 96–108.
Wittmeyer, J., Joss, L. & Formosa, T. (1999). *Biochemistry*, **38**, 8961–8971.
Woolfe, A. P. (1999). *Chromatin Structure.* New York: Academic Press.